

Nine-component refraction statics survey

D. C. Lawton

ABSTRACT

A 9-component refraction seismic survey was conducted near Calgary. A steel hammer striking a wooden beam was used to generate S waves, and a seisgun was used to produce P waves. Data were recorded on single 3-component geophones. Good quality P, SV and SH refracted data were acquired. The water table was found to produce strong P-wave refracted arrivals but was transparent to S waves. V_p/V_s below the water table was greater than 8. Static corrections to the base of the weathered layer at a depth of 20 m were 40 ms for P-P data, 89 ms for P-SV data, and 138 ms for SH-SH data. Weak shear-wave velocity anisotropy was found in unweathered Cretaceous clastic rocks in the study area.

INTRODUCTION

Recently, there has been increased interest in the use of multi-component reflection seismic data for the exploration and development of hydrocarbon reservoirs. In particular, three-component recording has enabled shear-wave reflection data to be collected (Domenico and Danbom, 1986). These data are, in the absence of subsurface anisotropy, either pure shear (SH-SH), or mode-converted (P-SV), recorded with transverse or radial geophones, respectively.

Static corrections are time corrections which are applied during the processing reflection seismic data to remove the effects of topography and near-surface velocity variations (weathering). In Alberta, the weathering statics problem is particularly severe due to the irregular thickness of glacial sediments which blanket most of the western Canada basin. This has a direct impact on the recording and processing of shear-wave reflection data because the velocity of shear-waves in the weathering layer is much less than that of compressional waves (Wiest, et. al., 1984; Anno, 1986). This results in much larger static corrections for S-wave data than for P-wave data.

The weathering statics problem in conventional P-wave data is generally solved by the analysis of head-wave arrivals ('first breaks'), obtained either from production reflection records or from separate 'weathering' surveys. Refraction analysis using these data is undertaken using delay time methods (Gardner, 1939; Hagedoorn, 1959; Hawkins, 1961; Palmer, 1980), or some type of forward-modelling or least-squares inversion scheme (Hampson and Russell, 1984) to provide the depth and velocity structure of the near surface layers. Static corrections are then computed by essentially 'replacing' these layers, to a specified datum, by material with a velocity equal to that of the deepest refractor (sub-weathering). The accuracy of refraction analysis is linked directly to the quality of the time picks of the headwave arrivals. Precise time picks for every trace yields reliable short and long wavelength statics solutions (Lawton, 1989), whereas average slope and intercept time methods provide only the long-wavelength component.

Good quality P-SV reflection data can now be collected routinely and this approach to obtaining shear-wave information appears to be favoured over SH-SH surveys. This is primarily because of the difficulty in efficient coupling of shear-wave sources to the ground, and the fact that P-P and P-SV surveys use a common source, whereas SH-SH

surveys require a different source. Furthermore, the SH-SH weathering static corrections are greater than those for P-SV surveys because in the former case, both downgoing and upgoing waves are S-waves, whereas in the latter case, the downgoing wave is a P-wave, with consequently a smaller associated static correction.

A problem with P-SV surveys is the difficulty of evaluating receiver static corrections. This is because a significant amount of P-wave energy is recorded by the radial geophones and SV-headwaves (either source-generated or mode-converted) are lost in P-wave multiple refractions. A common practice is to estimate the S-wave weathering static correction by simply multiplying the P-wave weathering static correction by a factor based on an assumed P-wave to S-wave velocity ratio for the near-surface sediments.

The purpose of this study was to estimate V_p/V_s for surficial glacial sediments near Calgary and to determine the ratio between the P-wave and S-wave weathering static corrections in the study area. This was achieved by undertaking an experimental multi-component refraction survey.

FIELD PROGRAM

The multi-component refraction test was undertaken during the 1989 University of Calgary Geophysics Field School, which was held at Jumping Pound (Twp 25, Rge 5 W5), about 30 km west of Calgary. At the site, a thin layer of glacial sediment covers sandstones and mudstones of the Cretaceous Belly River Formation.

Two different sources were used for the test. The shear wave source was provided by Unocal Canada Ltd. and consisted of an 80 kg steel hammer which struck the end of a 0.3 m x 0.3 m wooden beam. The beam was held down by a 1-ton cable truck and anchored to the ground by strips of angle iron. The hammer length was adjustable and pivoted from a wooden support beam which was lashed across the top of the cage on the cable truck. A photograph of the field set-up in operation is shown in Figure 1. For each shot, the hammer was raised manually to a fixed height, and released on command. Bouncing of the hammer on the end of the beam was prevented by catching it with a rope. The P-wave source used in the experiment was a Betsy seisgun (Varsek and Lawton, 1985).

Single three-component OYO geophones were used to acquire the data, with a group interval of 15 m. The geophone elements had a resonant frequency of 10 Hz and the geophone case was equipped with a levelling bubble and arrows for orientation, as shown in Figure 2. To minimise wind noise, the geophones were buried below the ground surface. A 48-trace DFS-III system was used to record the data, allowing 16 live ground stations for the active spread. When recording data with the S-wave source, the instruments were triggered by a geophone positioned on the wooden beam; the P-wave seisgun fired electric shells and was triggered using an Input-Output blaster.

Reciprocal records into a single spread were acquired in the experiment, with source locations coincident with the first and last geophones of the spread. At each source location, 5 data sets were obtained, consisting of 1 set of records using the P-wave source, and 4 sets of records using the S-wave source. A total of 150 records were acquired, with each data set consisting of 15 individual records which were vertically stacked to enhance the signal to noise ratio. The S-wave source was oriented in two orthogonal modes, firstly, transverse to the receiver spread to generate SH waves, and secondly, in-line with the spread to produce SV waves. In each of these modes, separate data sets were acquired with the hammer striking opposite ends of the beam.

During initial data collection using the S-wave hammer, a severe noise spike was observed across the records, coinciding with the shot time break. The source of this noise spike was eventually attributed to electromagnetic induction into the seismic cable, probably caused by the hammer becoming magnetised from repeated impacts. This problem was

ameliorated by uncoiling the seismic cable and moving it away from the vicinity of the source.

DATA REDUCTION

After demultiplexing the data, the 15 records from each data set were vertically summed. It was found that the time break was not consistent, but varied by up to 10 ms from shot to shot. For all data sets, the first record from that set was selected as the pilot record and each remaining record in the data set was cross-correlated with the pilot record. The lag for maximum correlation was then applied as a bulk shift to the record before summing.

The S-wave source invariably created some P-wave energy during operation because the wooden beam was rarely perfectly level and the hammer was not necessarily exactly orthogonal to the beam when it struck the end. The signal to noise ratio of the S-wave data was enhanced considerably by subtracting the data sets acquired with the hammer striking the opposite ends of the beam while in the same mode (transverse or radial). The S-wave energy has opposite polarity between the data sets, whereas the P-wave energy has the same polarity (Hasbrouk, 1987). Thus, when the data sets were subtracted, the S-wave energy was summed whereas the P-wave energy was attenuated. Prior to subtraction, the record pairs were cross-correlated to extract any residual time break error, and the average amplitudes of the records were also normalised.

After subtraction, the total data set was reduced to 6 records, consisting of 3 records from each end of the spread with vertical, transverse and radial source orientations.

RESULTS

Figure 3 shows an example of the final record obtained with the transverse source positioned at the eastern end of the spread. For ease of display, the 48-trace record was decomposed into three separate 16-trace records, containing the transverse, radial and vertical components of the recorded data, as indicated in Figure 3. The data in Figure 3a have been trace-equalised and scaled using a 500 ms sliding window. The transverse component contains the best data, as expected, since this record was acquired with the source in the SH mode. However, there is also considerable coherent energy on both the radial and vertical components. Figure 3b shows the same data displayed with only a constant scalar multiplier applied, so that the relative amplitude levels between the components can be better appreciated. This display shows that the radial component indeed has a similar amplitude level as the transverse component. Polarization studies will be undertaken to determine whether this observation indicates near-surface anisotropy, or whether there is coupling between the horizontal elements of the OYO geophones. Figure 3b shows that the true amplitude level of coherent energy on the vertical component is much lower than on either of the two horizontal components.

Figure 4 contains the same data as shown in Figure 3, and shows a comparison between subtracting and adding S-wave data set pairs with the same source orientation (transverse) but with opposite directions of excitation. Figure 4a shows results after subtracting the records, whereas Figure 4b shows the same data but after addition of the records. This results in attenuation of S-wave energy and enhancement of the P-wave energy, as shown by the significant P-wave refracted arrival on the vertical component. Some low-level P-wave energy is evident on the radial component, and the transverse component shows only surface-wave energy and a small residual SH refraction. Figure 4 illustrates the importance of the subtraction and addition processes for P and S wavefield separation.

NEAR-SURFACE VELOCITY STRUCTURE

Refraction analysis of the 6 processed records was undertaken to compare the near-surface P- and S-wave velocity and depth profiles. Matching source-receiver orientations from each of the records (SH-transverse; SV-radial; P-vertical) were sifted from the full 9-component data set to facilitate interpretation and display. These subsets are shown in Figures 5 and 6, for source positions at the eastern and western ends of the spread, respectively. Direct and refracted arrivals are marked on each record. The vertical-component records show a P-wave refracted arrival across all traces, whereas the transverse-component and radial-component records show a distinct crossover at an offset of about 60 m (4 traces).

Because of the limited source-receiver offset range and the lack of apparent refractor structure for both P and S data, a simple slope and intercept time interpretation was undertaken. Velocities and layer thicknesses, averaged from reciprocal records, are given in Tables 1 and 2, for S-wave and P-wave data respectively. A determination of the SV velocity in the surface layer was not obtainable from the radial-component records because of contamination of the near-offset data by P-wave energy (Figures 5, 6). This is considered to be caused by a probable asymmetric in-line radiation pattern of SV energy from the S-wave source when oriented in the radial direction. However, this was indeed fortuitous because no direct P-wave arrivals were observed on the vertical-component records and this enabled the P-wave velocity of the surface layer to be determined.

Table 1: Shear wave depth and velocity structure

Layer	SH		SV	
	Velocity (m/s)	Thickness (m)	Velocity (m/s)	Thickness (m)
1	295 ± 10	20 ± 2	Not determined	$18 \pm 2^*$
2	1330 ± 30	-	1200 ± 40	-

* Thickness calculation based on velocity of 295 m/s for layer 1.

For the P-wave results in Table 2, the thickness of the second layer and the velocity of the third layer (3150 ± 50 m/s) were determined from first break analysis of records obtained from a conventional, P-wave seismic program which was run later along a line which included the test refraction spread.

Table 2: Compressional wave depth and velocity structure

Layer	Velocity (m/s)	P	Thickness (m)
1	600 ± 10*		10 ± 2
2	2450 ± 30		10 ± 3 ⁺
3	3150 ± 50 ⁺		—

* Determined from radial component record with SV source.

⁺ Determined from production P-wave records (1440 m spread length).

DISCUSSION

The data from Tables 1 and 2 are summarised in Figure 7, which shows clearly that the shallow velocity structures for P-waves and S-waves are very different. The results of this study are similar to those described by Wiest and Edelmann (1984) from a multi-component refraction survey in northern Germany. The increase in P-wave velocity at a depth of 10 m coincides approximately with the top of water-saturated sediment, probably weathered sandstone (shot-hole driller's log). No increase in S-wave velocity is evident at this interface, an observation which is consistent with velocity studies of porous rocks by Domenico (1976) and Gregory (1976). Note that V_p/V_s increases to a value greater than 8 in the water-saturated, weathered zone.

Generally, the quality of the radial-component data (SV) was not as good as that of the transverse-component data (SH). However, the SV-wave velocity in the deepest refractor appears to be about 10% lower than the SH-wave velocity (horizontal propagation direction), indicating that the unweathered Cretaceous sediments below the test line are anisotropic.

The differences in the near-surface P-wave and S-wave velocity structure has a significant impact on weathering static corrections. Figure 7 shows the magnitude of the static corrections which would be applied in P-P, P-SV and SH-SH reflection surveys. These values were computed on the basis of vertical travelpaths and to a datum at a depth of 20 m below surface. The total weathering static for the SH-SH survey is 3.5 times greater than the P-P static, and the P-SV static is over twice the value of the P-P static correction. If these differences are not taken into account during the processing of converted S-wave data, then the converted-wave reflections will lag the P-wave reflections when correlations between vertical and radial-component stacked sections are made.

CONCLUSIONS

The following conclusions are drawn from this study:

1. In the study area, the low-velocity layer for S-waves is considerably thicker than that for P-waves.
2. Shear waves are unaffected by the water table whereas the P-wave velocity increases markedly at the water table.
3. The S-wave velocity of dry, surface sediments is about 295 m/s and the P-wave velocity is about 600 m/s.
4. Below the water table, at a depth of about 10 m, the P-wave velocity increases to over 2400 m/s while the S-wave velocity remains low, resulting in a V_p/V_s of greater than 8.
5. The base of weathering occurs at a depth of about 20 m, for both P and S waves.
6. Weak shear-wave velocity anisotropy was found for the unweathered rocks.
7. Static corrections to a datum at the base of weathering were computed to be 40 ms for P-P data, 89 ms for P-SV data, and 138 ms for SH-SH data.

ACKNOWLEDGEMENTS

I wish to thank Mr. Scott Graham from Unocal Canada for providing us with the components for the shear-wave source.

REFERENCES

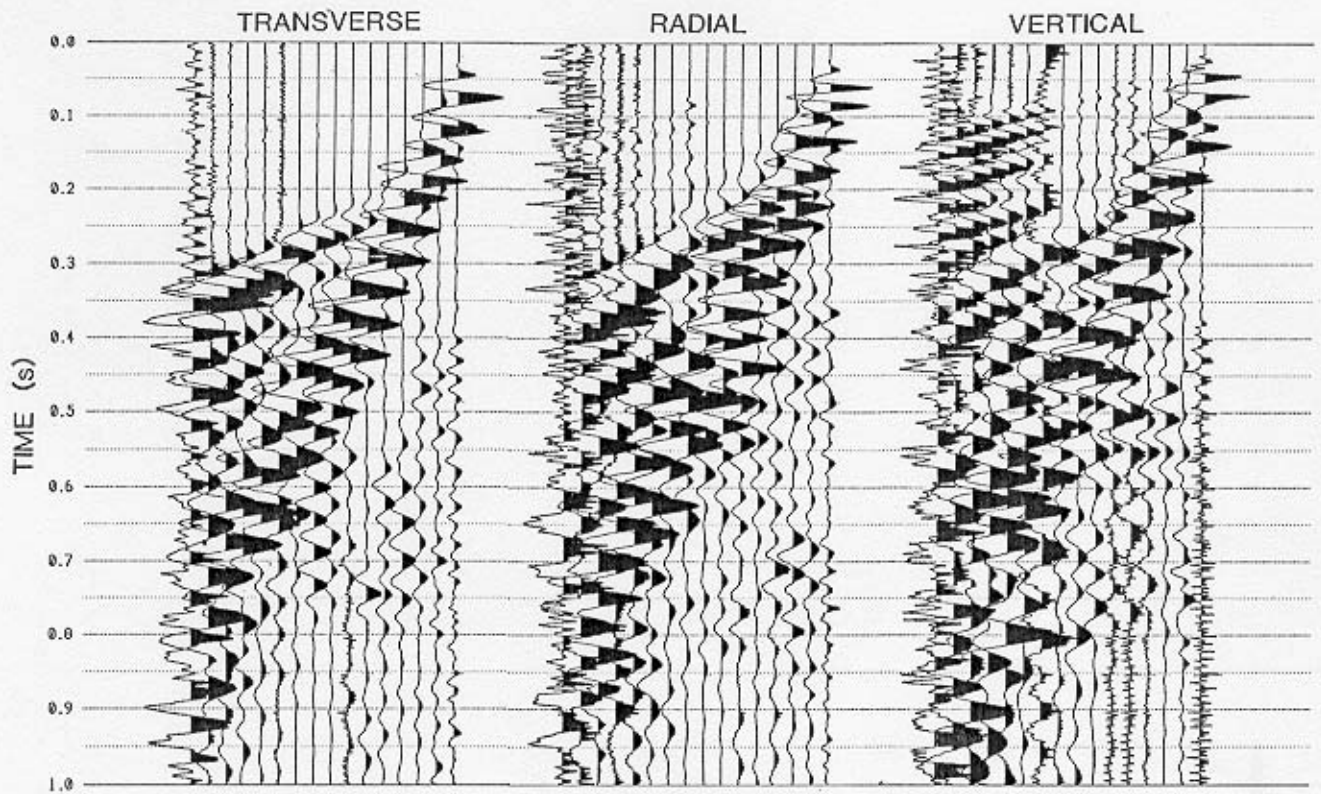
- Anno, P. D., 1987, Two critical aspects of shear-wave analysis: statics solutions and reflection correlations: in Danbom, S. H. and Domenico, S. N. (editors), shear-wave exploration, Society of Exploration Geophysicists Geophysical Development Series, Vol. 1, 48-61.
- Domenico, S. N., 1976, Effect of brine-gas mixture on velocity in an unconsolidated sand reservoir: Geophysics, 41, 882-894.
- _____, and Danbom, S. H., 1987, Shear-wave technology in petroleum exploration - past, current, and future: in Danbom, S. H. and Domenico, S. N. (editors), shear-wave exploration, Society of Exploration Geophysicists Geophysical Development Series, Volume 1, 3-18.
- Gardner, L. W., 1939, An areal plan of mapping subsurface structure by refraction shooting: Geophysics, 4, 247-259.
- Gregory, A. R., 1976, Fluid saturation effects on dynamic elastic properties of sedimentary rocks: Geophysics, 41, 895-921.
- Hagedoorn, J. G., 1959, The plus-minus method of interpreting seismic refraction sections: Geophysical Prospecting, 7, 158-182.
- Hawkins, L. V., 1961, The reciprocal method of routine shallow seismic refraction investigations: Geophysics, 26, 806-819.
- Hampson, D., and Russell, B., 1984, First break interpretation using generalised linear inversion: J. Soc. Expl. Geophys., 20, 40-54.
- Hasbrouk, W. P., Hammer-impact, shear-wave studies: in Danbom S. H. and Domenico, S. N. (editors), shear-wave exploration, Society of Exploration Geophysicists Geophysical Development Series, Volume 1, 97-121.
- Lawton, D. C., 1989, Computation of refraction static corrections using first-break traveltime differences: Geophysics, 54, 1289-1296.
- Palmer, D., 1980, The generalised reciprocal method of seismic refraction interpretation: Soc. of Expl. Geophys..
- Varsek, J. L., and Lawton, D. C., 1985, The seisgun - Part 1: field tests J. Can. Soc. Expl. Geophys., 21, 64-76.
- Wiest, B., and Edelmann, H. A. K., 1984, Static corrections for shear wave sections: Geophys. Prosp., 32, 1091-1102.



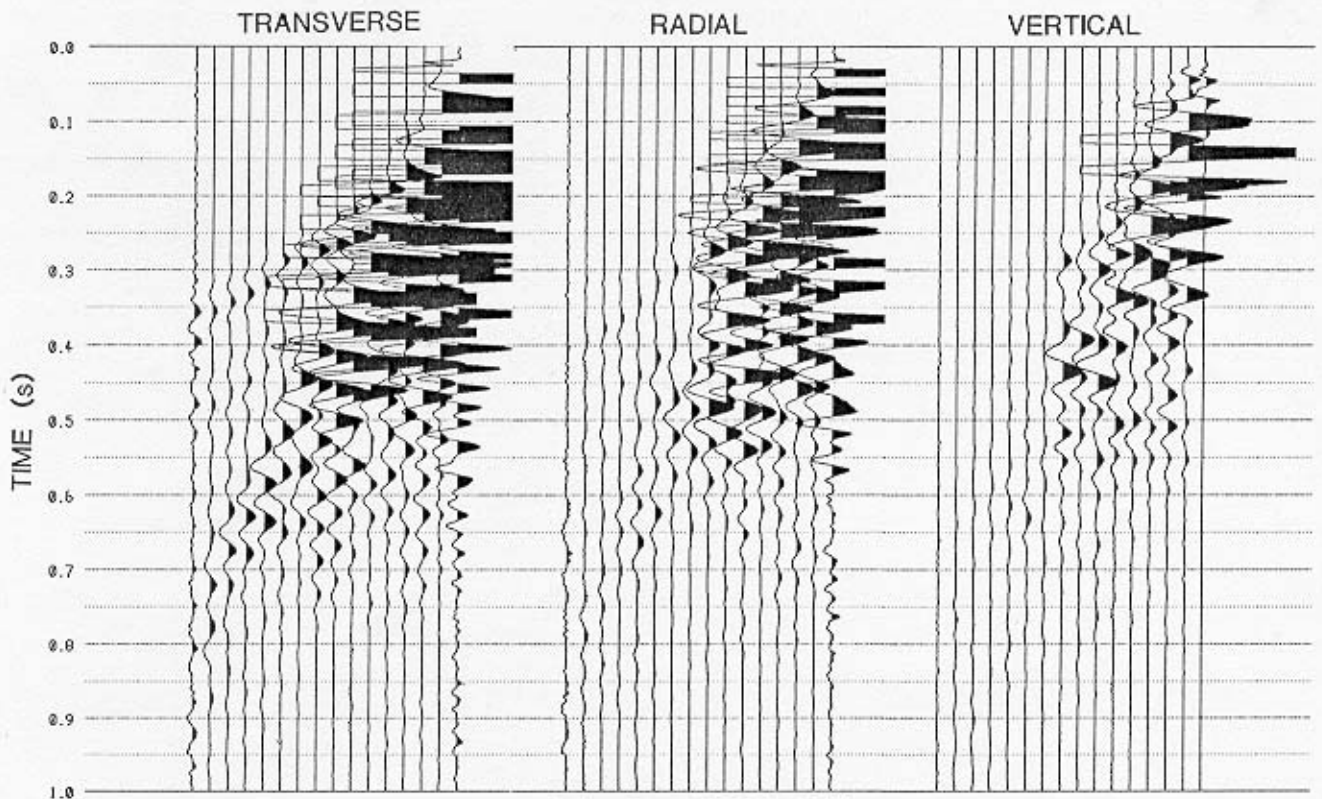
FIG. 1. The shear-wave source in operation.



FIG. 2. A 3-component OYO geophone in position, showing the leveling bubble and orientation arrows.



(a) SH SOURCE



(b) SH SOURCE

FIG. 3. Processed 3-component record obtained with the shear source in the SH mode at the eastern end of the spread: (a) trace-equalised with a 500 ms agc; (b) scalar multiplier only.

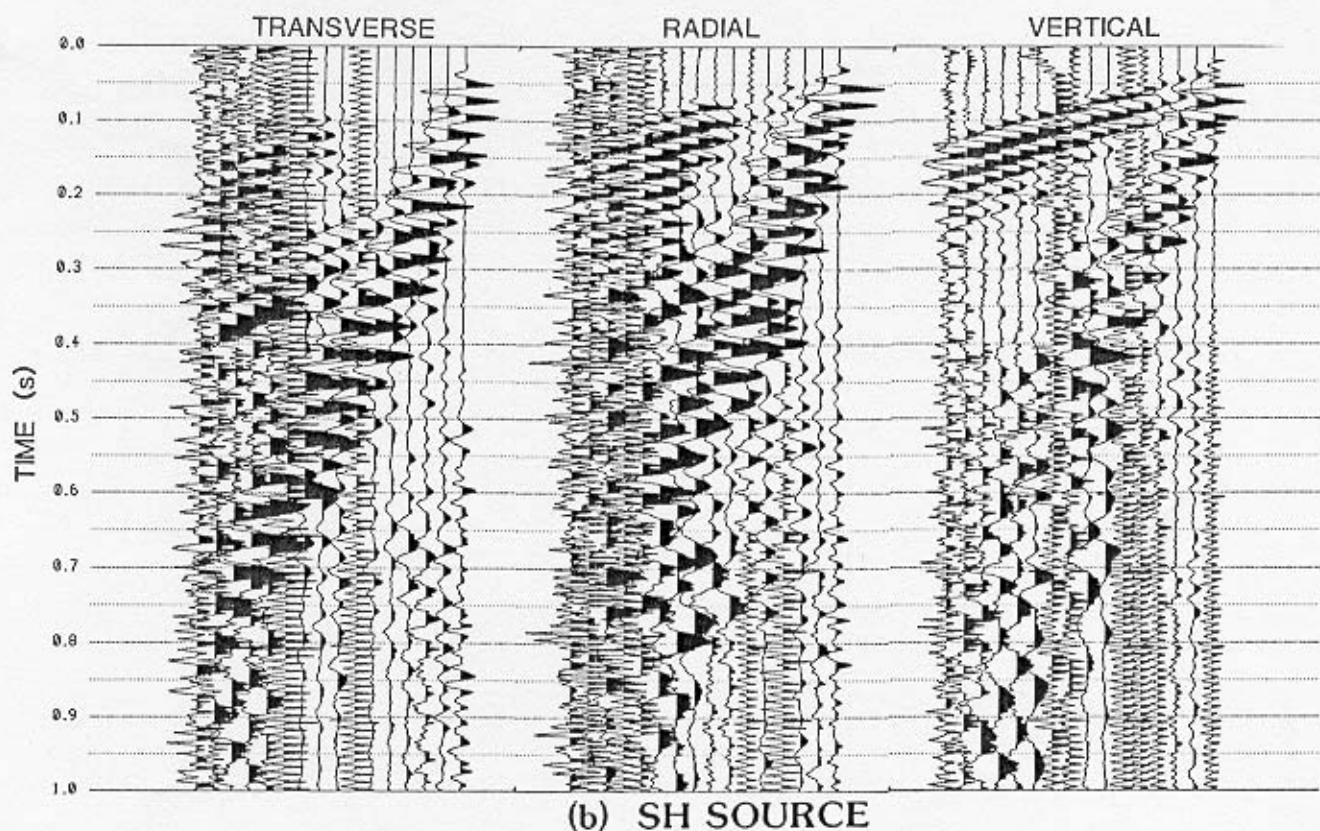
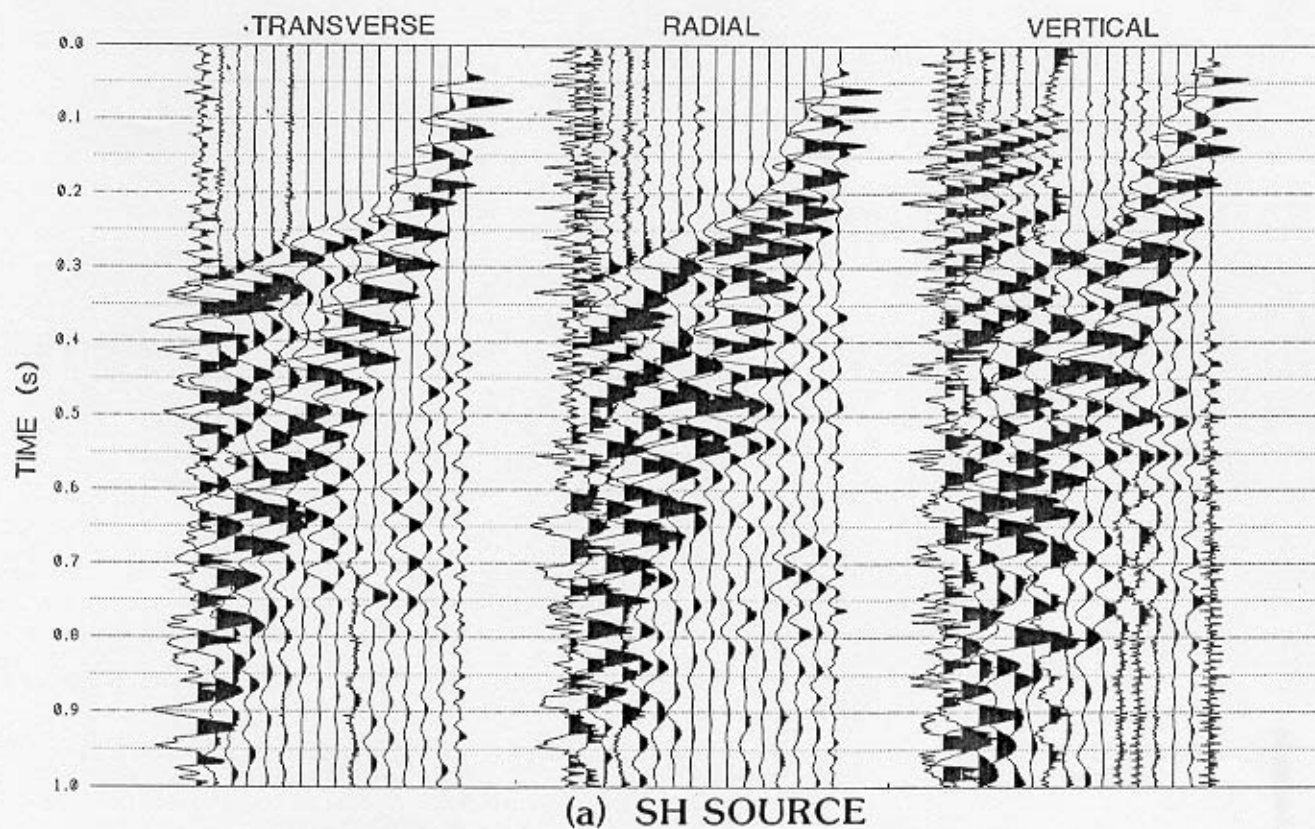


FIG. 4. Comparison of : (a) subtracting records with opposite directions of source excitation, and (b) adding records with opposite direction of source excitation. Source was located at the western end of the spread, in the SH mode.

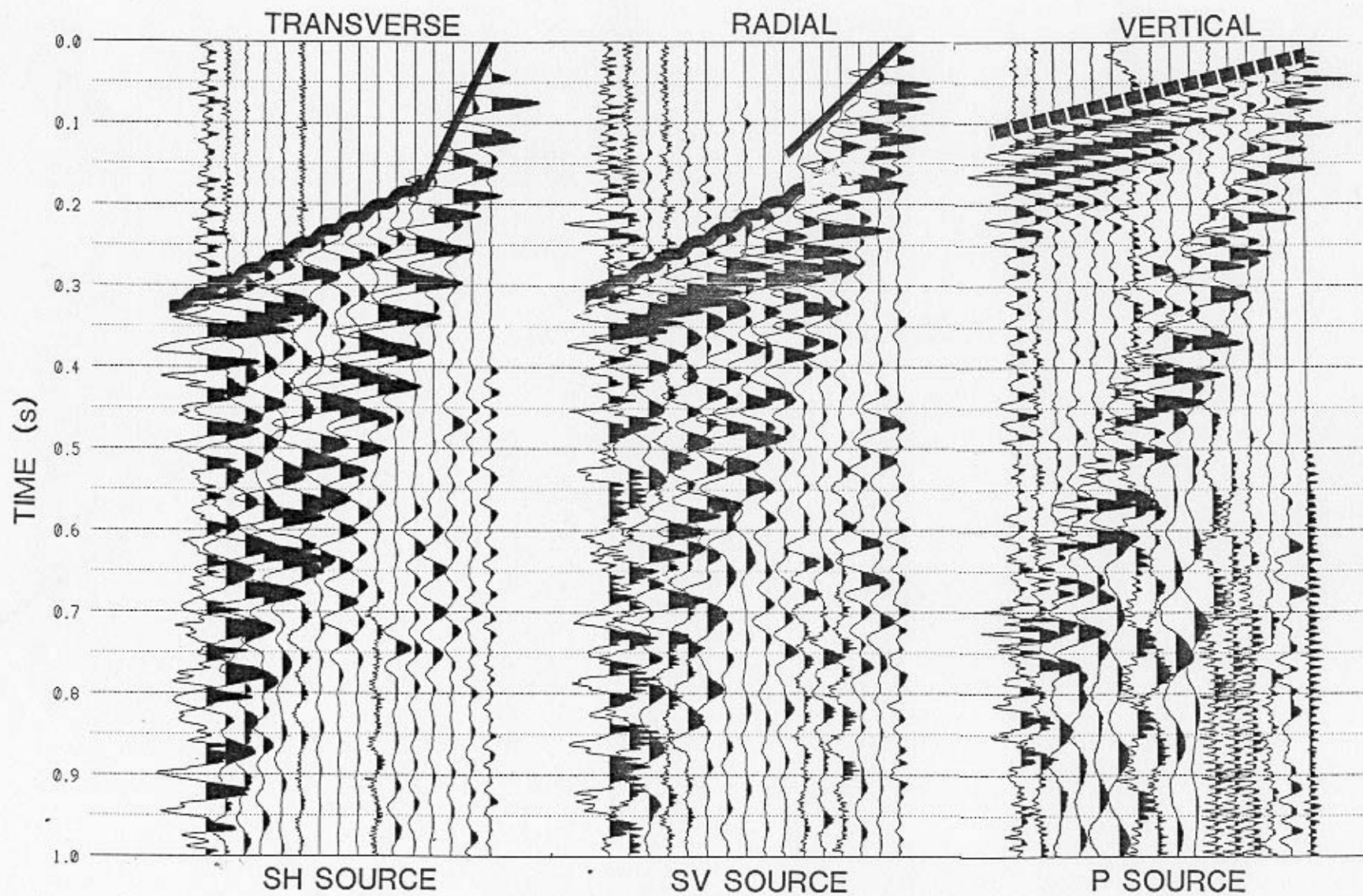


FIG. 5. Processed records for the source located at the eastern end of the spread. Direct and refracted arrivals are marked.

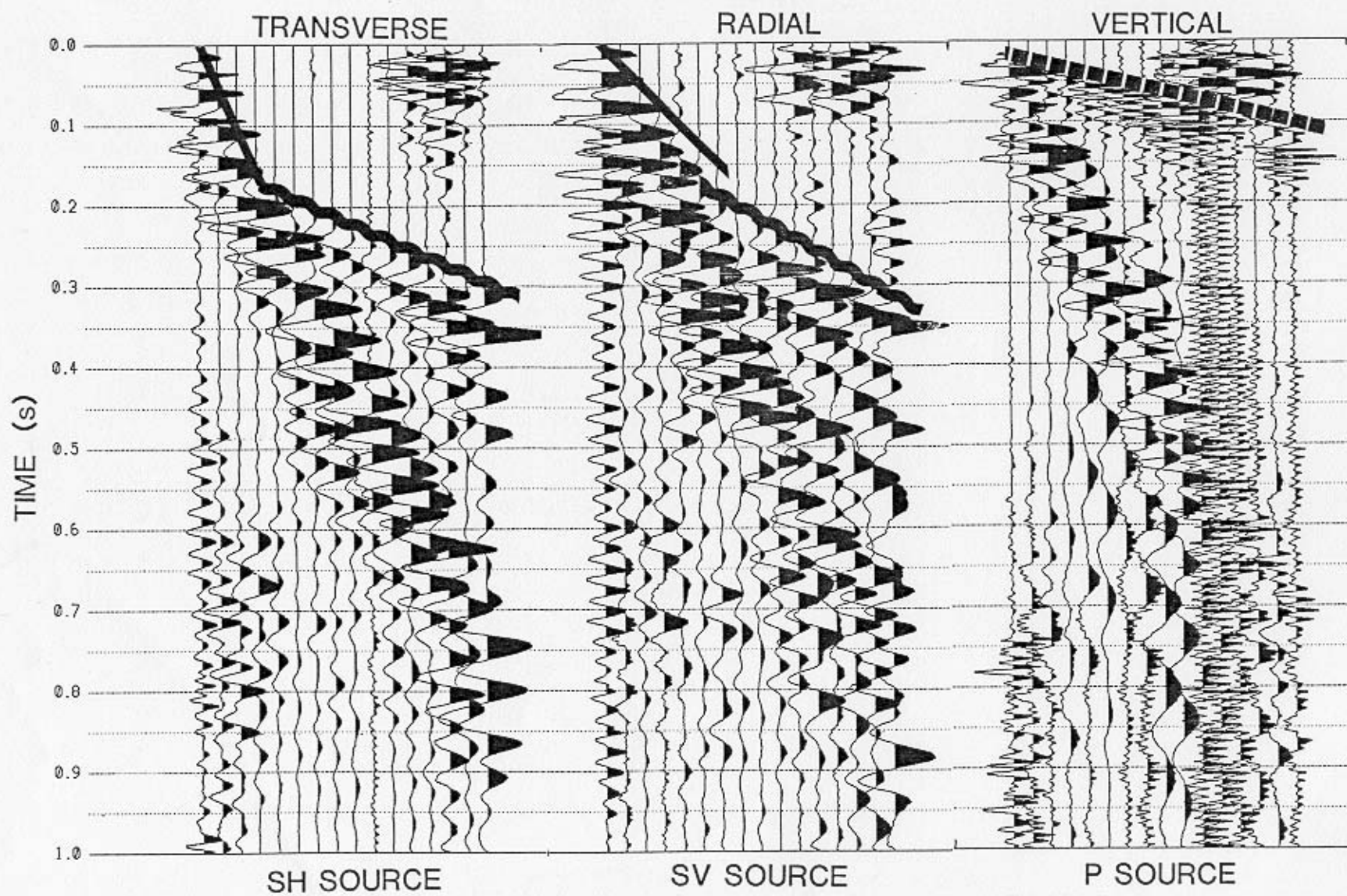


FIG. 6. Processed records for the source located at the western end of the spread. Direct and refracted arrivals are marked.

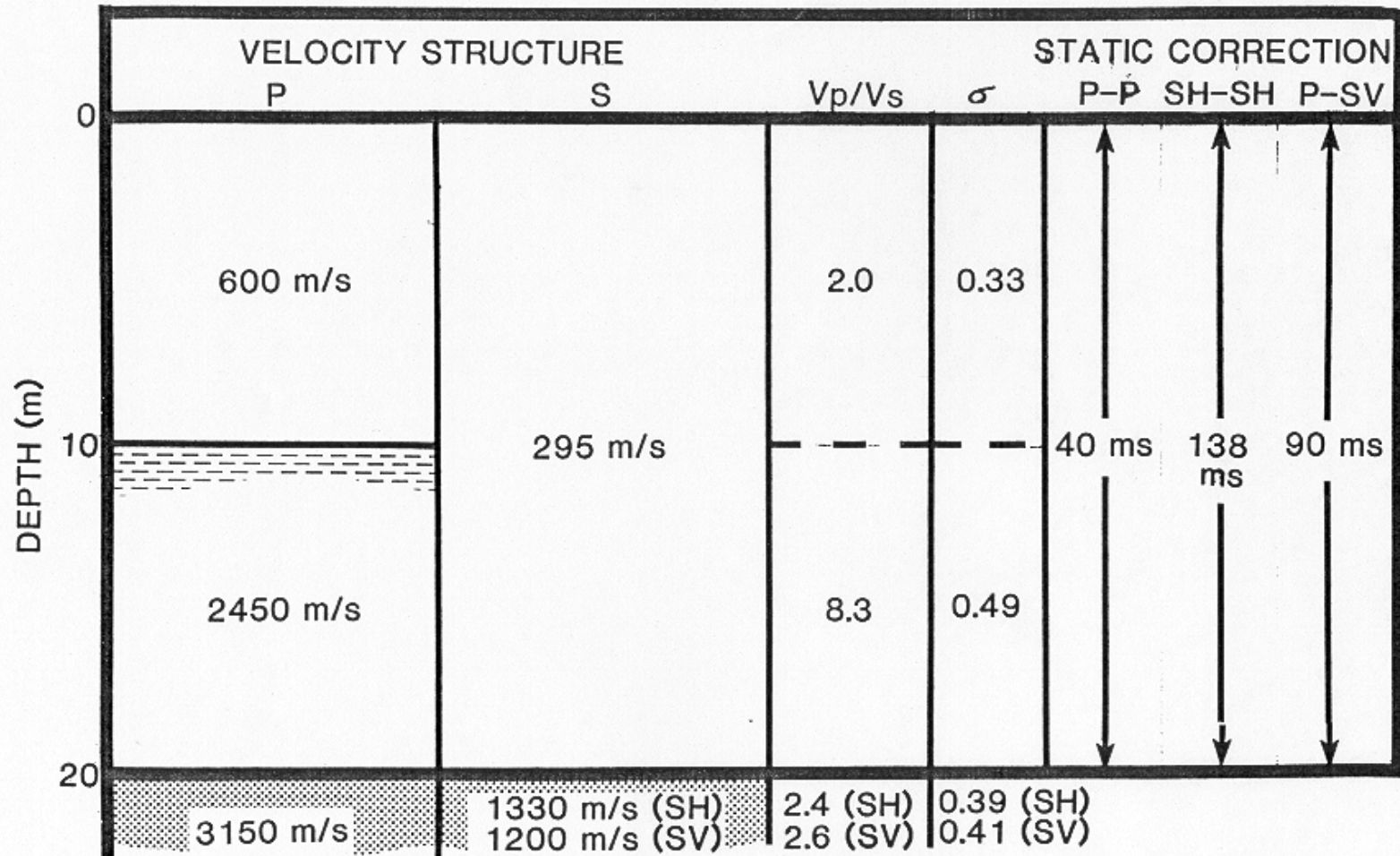


FIG. 7. Summary of the near-surface P-wave and S-wave velocity structures at Jumping Pound.